Archaeological analogues for the verification of lifetime models of containers for deep radioactive waste repositories

Authors: Jan Stoulil et al.

SÚRAO

AUTHORS: Stoulil J.[1], Mukhtar S. [1], Lhotka M. [1], Bureš R. [1], Kašpar V. [2], Šachlová Š.[2], Pecková A.[2], Havlová V.[2], Danielisová A.[3], Malyková D.[3], Barčáková L.[3], Machová B.[3], Březinová H.[3], Ottenwelter E.[3], Němeček J.[4], Němeček J.[4]

University of Chemistry and Technology, Prague (VŠCHT Praha)[1], ÚJV Řež[2], Institute of Archaeology of the Czech Academy of Sciences (Archeologický ústav AVČR)[3], Faculty of Civil Engineering CTU Prague (FSv ČVUT)[4]

Lucie Hausmannová

Project manager (SÚRAO)

Date

Jan Stoulil

Project manager (VŠCHT Prague)

Date

SÚRAO

SÚRAO

Contents

List of attachments

Attachment 1 – Geographical locations and dating of the sites

Attachment 2 – Pedological evaluation of soils from the sites and geochemical modelling

Attachment 3 – Data for the evaluation of corrosion attack and estimation of the lifetime

Attachment 4 – Evaluation of the mechanical properties of the corrosion products

List of abbreviations:

BaM	commercial name of bentonite (bentonite and montmorillonite)
BCV	commercial name of bentonite (Černý Vrch bentonite)
BET	method for the determination of porosity using the Braunauer-Emmett-Teller gas adsorption isotherm
BSE	back-scattered electron detector (SEM imaging method)
EDS	energy dispersive X-ray spectroscopy (SEM elemental analysis)
SBPOW	synthetic pore water; the term used for the artificial BaM bentonite pore solution considered in the waste disposal package project
SE	secondary electron scan (SEM imaging method)
SEM	scanning electron microscopy
WDP	waste disposal package
XRD	X-ray diffraction

Abstrakt

V rámci projektu bylo studováno přes 200 artefaktů z 15 lokalit. 4 z lokalit byly svým významem klíčové, protože se jednalo o dna rybníků s trvalým zavodněním. Půdy na všech lokalitách byly tvořeny hrubšími částicemi než bentonity a postrádaly vlastnost bobtnání. Z chemického hlediska se však pórové roztoky půd z lokalit velmi podobaly bentonitovým. Lišily se hlavně v kationtovém složení, aniontové však bylo podobné, což je pro korozní chování klíčové. Prostředí nebylo úplně anaerobní, což se projevilo na složení korozních produktů. Hlavní složkou byly oxidy a oxohydroxidy. Pro vznik uhličitanových korozních produktů, detekovaných v dřívějších laboratorních i *in situ* experimentech jiných projektů, je potřeba velmi nízkých oxidačně-redukčních potenciálů, tedy úplně anaerobního prostředí. Přesto však byl transport kyslíku pomalý a podíl aerobní koroze vůči anaerobní zanedbatelný. Hodnocení archeologických artefaktů odhalilo velmi významný faktor, podílející se na mechanismu korozního napadení v pozdější fázi uložení v půdním prostředí. Zatímco v první fázi uložení se dochází k postupnému zaplňování pórového systému bentonitu precipitujícími korozními produkty a postupnému zpomalování korozního napadení, v druhé fázi je již transport železnatých kationtů omezen příliš, precipitace korozních produktů je významně posunuta na rozhraní s kovem a nově vznikající korozní produkty způsobují mechanické porušení korozních produktů ve vnějších vrstvách. K tomuto porušování pak dochází cyklicky i dále. Mechanické vlastnosti korozních produktů jsou totiž velmi chabé, tyto jsou snadno deformovatelné a velmi pórovité. Ukončený projekt tak odhalil velmi závažný fakt, nezbytný pro správné určení životnosti UOS, který nebyl na základě krátkodobých dat odhalitelný.

Klíčová slova

archeologické analogy, transport, korozní produkty, životnost UOS

Abstract

More than 200 artifacts from 15 localities were studied within the scope of this project. 4 localities were crucial, because those were pond beds with continual flooding. Soils at all localities were coarser compared to bentonites and lacked swelling ability. Pore solutions of the soils were very similar to bentonite pore solutions. They differ in cation composition, but anion composition was similar, which is more important for corrosion behaviour. The environment was not completely anaerobic, what influenced the composition of corrosion products. The compounds were oxides and oxohydroxides. Very low oxidation-reduction potential (fully anaerobic environment) is necessary for the formation of carbonate-based corrosion products, that were detected as major corrosion products in the previous lab and *in situ* experiments on another projects. Nevertheless, the oxygen transport was very slow and the contribution of aerobic corrosion was negligible compared to anaerobic corrosion. The evaluation of archaeological artifacts revealed very important factors influencing corrosion mechanism in latter stage of soil burial. Precipitation of corrosion products is a driving phenomenon for transport limitation and decrease of corrosion rate in the early stage of burial, while the ferrous species transport is limited extensively within the latter stage resulting in mechanical stress of outer corrosion products layers to previously formed corrosion products and subsequent cracking. This mechanical damage is repeated in the cycle. The mechanical properties of corrosion products are poor, they are easily deformable and very

porous. The project has revealed a very important phenomenon, necessary for the right lifetime estimation, which would not be obvious based on the short-term experiments data.

Keywords

Archaeological analogues, transport, corrosion products, WDP lifetime

1 Evaluation of the archaeological sites

15 archaeological sites with an age of 500 to 2600 years were opened and over 200 artifacts were evaluated. Details regarding the geographical location of the sites and their archaeological dating can be found in Appendix 1 (a list of minimum dating is also given in Tab. 2).

Tab. 1 summarises an overview of the samples. All the discovered artifacts were analysed using X-ray imaging. It was possible to obtain fragments of the fallen corrosion products from a minor part of the samples. Some samples with lower historical values were provided to obtain corrosion products covering the full thickness of the layer and ability to study on perpendicular sections.

Tab. 1 Overview of the samples obtained from the sites

Site	Žehuň	Lítožnice	Xaverov	Jiviny	Vraňany	Velvary	Tuchoměřice	Utín
Number of artifacts subjected to X-ray imaging	15	25	2	8	4	2	2	14
Number of corrosion product samples	14	1	2	3	1	1	1	5
Number of samples with metal core for destructive analysis	14	1	2	1	0	0	1	0
Site	Slaný	Opatov	Kučeř	Konopiště	Čejkov	Chrbina	Chomutov	
Number of artifacts subjected to X-ray imaging	187	3	3	2	4	2	7	
Number of corrosion product samples	9	1	3	2	1	2	2	
Number of samples with metal core for destructive analysis	1	0	3	2	1	1	0	

The pedological and geochemical assessment of the sides is summarised in Appendix 2. Tab. 2 provides basic data on the sites. The youngest site is Kučeř (500 years old) and the oldest Slaný (2,600 years old). The minimum depth of the artifacts below the earth's surface ranged from 0.1 m (Tuchoměřice, Podmoky) to 1.2 m (Vraňany). Soil pore filling (based on the ratio of bulk moisture to porosity) reveals incomplete waterlogging at most sites. Only the Lítožnice, Xaverov, Jiviny and Žehuň sites (the bottoms of ponds) were are fully watered. These sites have constant

transport of oxygen to the surface of the artifacts all year around as well as a temperature maintains at an approximately constant level by the pond water column. The other sites, although wet, have cyclically variable oxygen transport due to the incomplete and seasonally variable water content of the soil pore system. Temperature can also fluctuate at sites with a lower depth of deposition.

Tab. 2 Basic characteristics of the sites and soils

Site	Min. age (a)	Min. deposition depth (m)	Porosity (% by volume)	Moisture (% by volume)	Pore filling (%)
KUCEŘ	500	0.20	36.3	15.6	43
KONOPIŠTĚ	550	0.15	41.4	24.8	60
CHRBINA	570	0.70	51.9	24.9	48
OPATOV	600	0.20	49.3	16.3	33
ČEJKOV	600	0.15	46.8	10.0	21
VRAŇANY	1000	1.20	46.1	23.0	50
CHOMUTOV	1300	0.50	40.9	36.5	89
VELVARY	1400	1.00	56.1	28.0	50
TUCHOMĚŘICE	1500	0.10	47.8	26.2	55
LÍTOŽNICE	1600	0.30	33.6	35.7	106
XAVEROV	2000	0.15	35.1	42.4	121
PODMOKY	2000	0.10	49.4	7.4	15
ŽEHUŇ	2100	0.25	43.9	45.0	103
JIVINY	2100	0.40	34.2	37.0	108
SLANÝ	2600	0.45	44.0	25.5	58

An example of particle coarseness assessment using sieve analysis is shown in Fig. 1. Detailed particle coarseness assessment values from all sites are given in Appendix 3. Technologically processed bentonite has a main fraction size of 100 – 45 µm by weight fraction. The soil from the Lítožnice site (and very similarly all the others) has histogram shifted towards larger particles; but when converted to particle size and number, the histogram is already comparable to that of the bentonite, although the total numbers are in order of magnitude lower and spread over more fractions, with the main fractions remaining 100 – 45 µm and 45 – 36 µm.
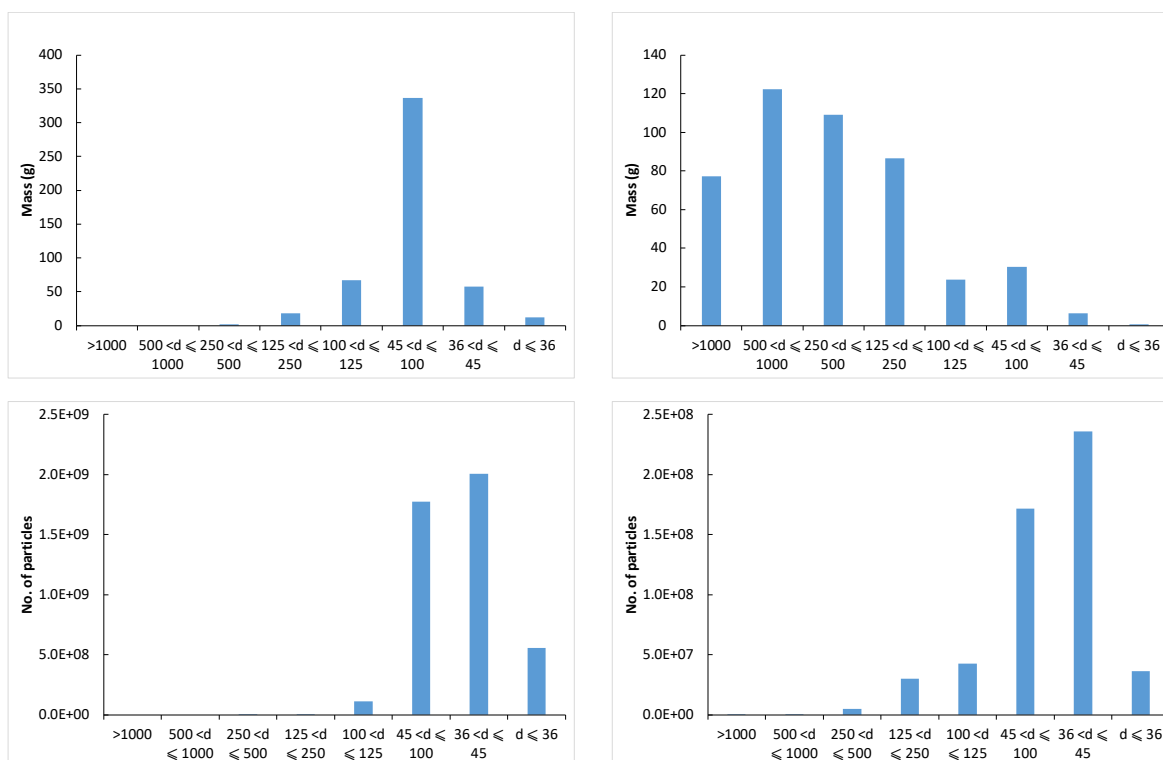

Fig. 1 Comparison of the sieve analysis of a BCV bentonite sample (left) and soil from the Lítožnice site (right): histogram of the mass fractions (top) and following conversion to particle counts (bottom)

The chemistry of pore solution soils differs from bentonite soils especially in the case of cations. Examples of compositions from 4 sites are shown in Fig. 2. Soil pore solutions are typically high in Ca, whereas bentonites dominate by Na and Mg. The anion composition is very similar to that of the bentonite pore solutions over a wide range of solutions from BaM (sulphate rich) synthetic bentonite pore water (SBPOW) to BCV bentonite (bicarbonate rich).
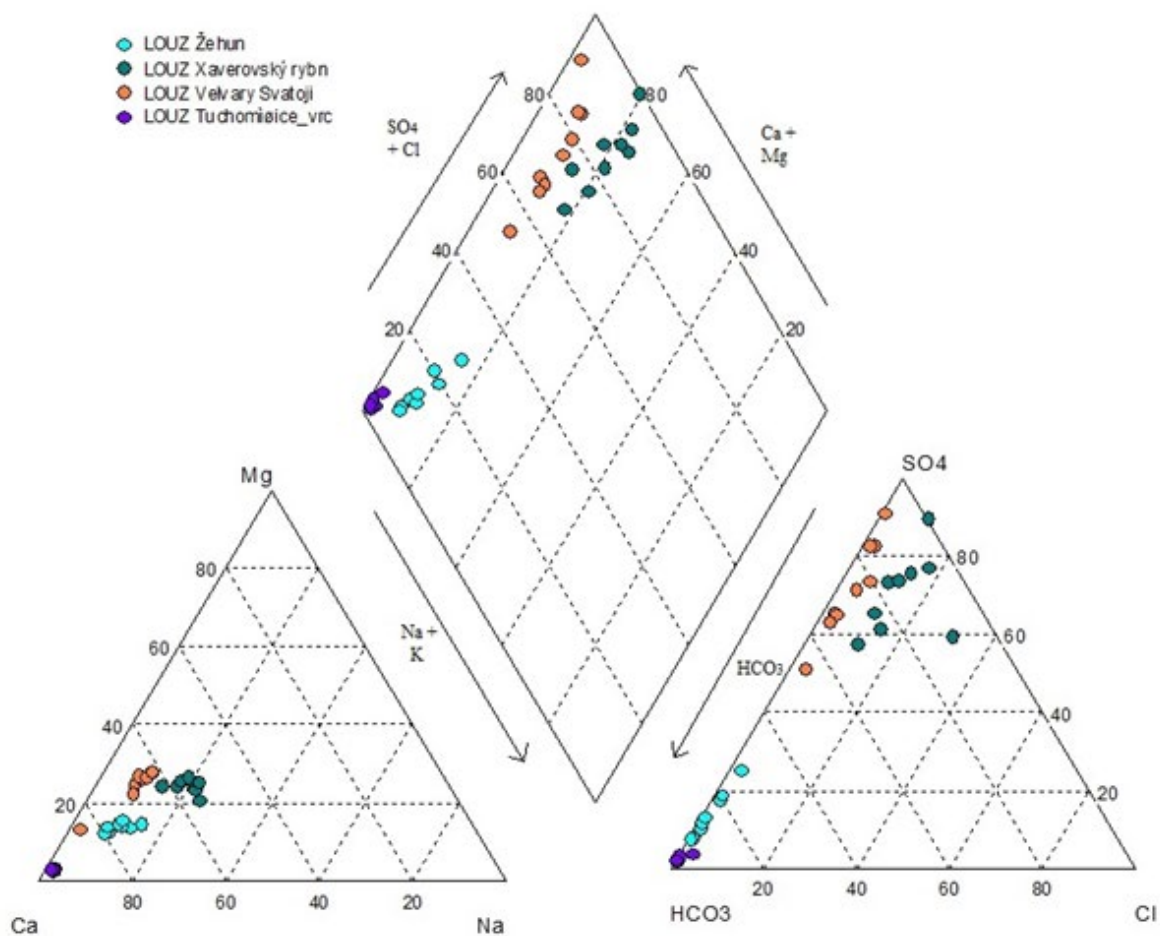
Fig. 2 Example of the composition of the soil pore solutions in the form of a Piper diagram

Thanks to long-term reclamation it was possible to collect soil pore solutions from the Lítožnice site throughout the year and perform analytical evaluations on an ongoing basis. At the other sites it was only necessary to carry out samplings once during a short-term opening of the site (archaeological survey, draining of the pond, etc.). The concentration of all components of the soil solution at the Lítožnice site was observed to fluctuate throughout the year. It exhibited no clear trend. The only trend observed (Fig. 3) was in chloride (higher in winter), bicarbonates and pH (higher in summer). It is, therefore, very likely that at other sites, soil pore solutions may also change in composition throughout the year and a single sampling may not be entirely telling.
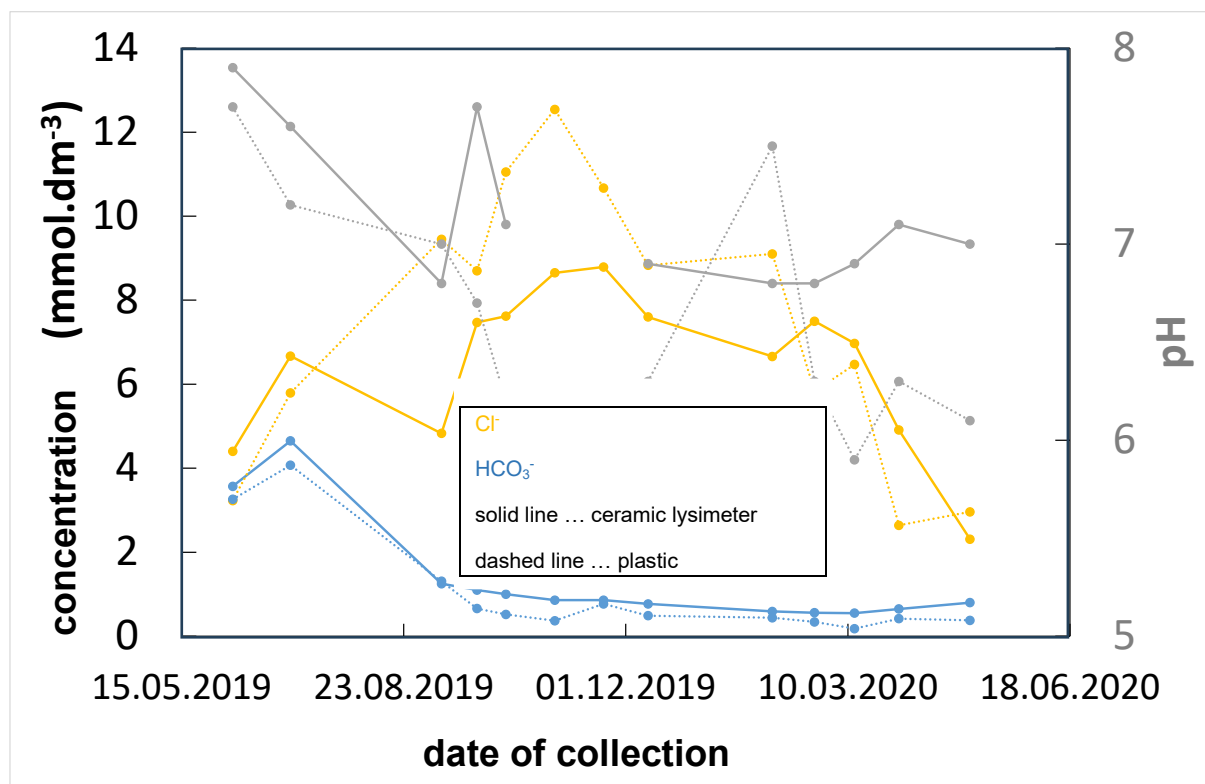
Fig. 3 Inter annutal trend of the concentration of chlorides, bicarbonates and pH of the soil pore solution at the Lítožnice site

An interesting feature is a very high content of dissolved silicates in the soil pore solution (see the summary in Fig. 4, with data from most sites). Even a concentration between 10^{-2} to 10^{-1} mmol.dm^{-3} didn't lead to a formation of silicate corrosion products, as described in detail in chapter 2.
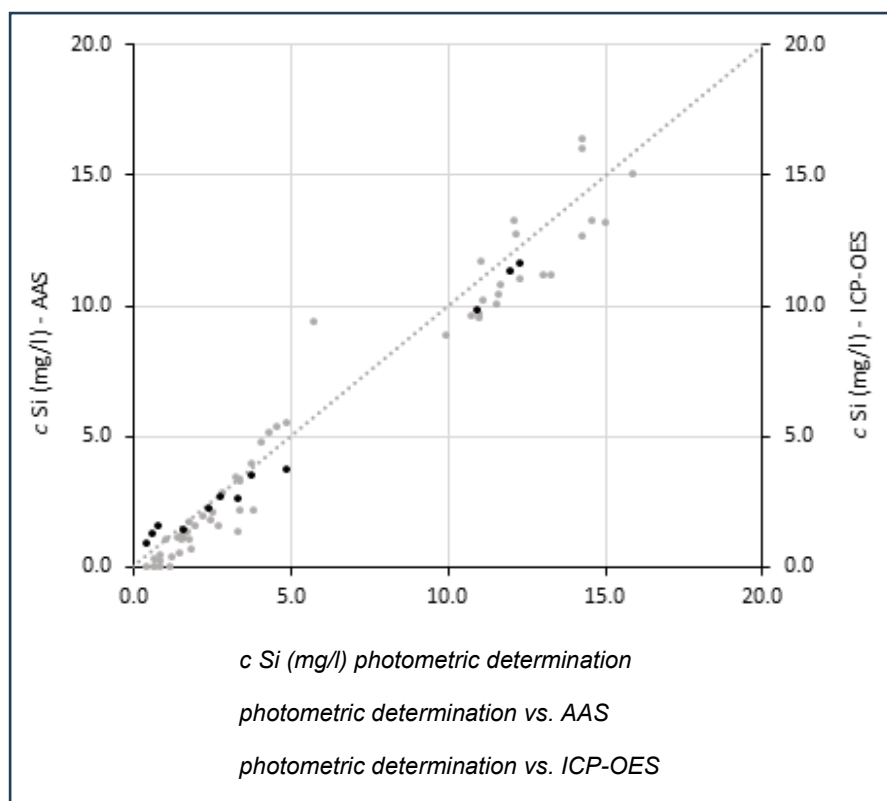
Fig. 4 Comparison of the determination of the silicate content using different methods

Geochemical modelling was performed for the determined soil pore solutions from the Jiviny, Xaverov, Lítožnice and Žehuň pond sites, as well as at the Slaný site, which has a high content of anaerobic magnetite (see Chapter 2). The input parameters for the modelling were 11°C (the average temperature of the upper layer of the soil) and 25°C (the temperature of extreme heating during the summer months). The concentration of Fe was set at two levels: 0.001 mol.dm^{-3} (corrosion supersaturation of the solution at the surface with the metal) and 0.0001 mol.dm^{-3} (solution depleted by the precipitation of the corrosion products).

The geochemical modelling indicated that $Fe(OH)_2$, magnetite, siderite and hematite comprised the main corrosion products. Examples of the phase stability diagrams as a function of Eh and pH are shown in Fig. 5. Silicates were also determined in the leach solutions, which was considered in the models. If dissolved silicates in solution are considered, solid silicate phases such as minnesotaite or croenstedtite appear in the diagram. Although they were not detected via the X-ray diffraction (see Chapter 2), it could not be excluded that they form a part of the corrosion products layer as an amorphous phase. No silicates were determined in the solutions obtained via high-pressure extraction; thus, the diagrams mainly include the above-mentioned corrosion products based on oxides and carbonates. The pH at the surface may be locally above 8 (as determined via the pH values of the soil pore solutions) due to alkalinisation by cathodic reaction. The main anaerobic corrosion product in the pH between 8 – 11 is magnetite and, at lower Eh values (completely anaerobic environments), siderite.
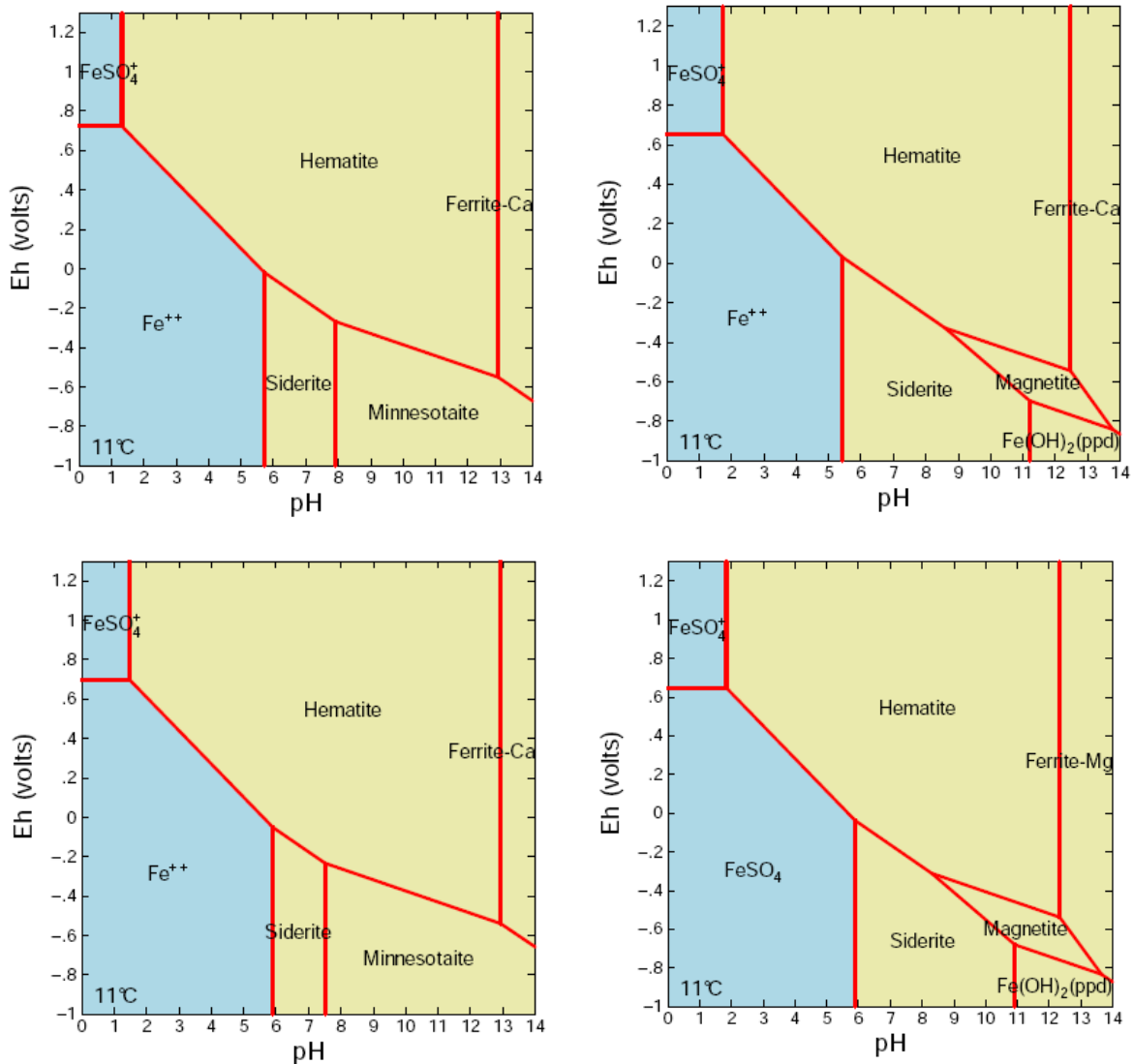
Fig. 5 Example of corrosion product stability diagrams at the Jiviny (top) and Xaverov (bottom) sites: solid sample leachate (left) and pressure extraction solution (right)

2 Evaluation of the corrosion products and the corrosion attack

The phase composition of the corrosion products was determined by X-ray diffraction. The layers commonly also contained particles of soil components. The semi-quantitative bulk composition of the represented phases was determined via the Rietveld analysis method. Detailed data obtained from all sites are provided in Appendix 3. An example of the composition of the corrosion products from the Žehuň site is provided in Tab. 3. The corrosion products correspond to the models in terms of the content of oxide and carbonate phases and, in addition to siderite, magnetite and hematite, they also contain goethite and lepidocrocite, which comprise kinetic precursors of hematite. In addition to soil particles, they also include iron compounds such as fayalite and wüstite, which are formed only at high temperatures. Thus, there must have already been a layer of scale on the surface of the artifacts. The unknown part of the magnetite thus belongs to this layer and does not represent a subsequent corrosion product formed during deposition; this renders the proposal of subsequent conversion to a layer of corroded iron debatable and is burdened with an unknown error. At other sites, the presence of scale in a thick layer affecting the results was not detected.

Tab. 3 Phase compositions of the corrosion product samples from the Žehuň site

ŽEHUŇ (% by volume)	Magnetite	Hematite	Goethite	Wüstite	Lepidocrocite	Siderite	Fayalite	Albite	Calcite	Microcline	Vivianite	Kaolinite	Rutile	Silica
Sample-002	2	--	19	--	--	4	--	8	8	8	--	--	--	--
Sample-005	1	--	--	--	--	21	--	8	3	--	14	--	1	52
Sample-010	--	--	--	--	--	7	--	2	8	--	13	--	--	70
Sample-012	17		18		--	13	--	7	9	--	--	--	--	35
Sample 2013-1	12	--	57		--	--	9	--	14	--	--	--	--	8
Sample 2013-4	15	7	52	1	--	--	--	--	16	--	--	--	--	9
Sample 2013-5	6	3	15	13	--	--	32	--	4	--	--	--	--	26
Sample 2012-1	4				--	2	--	6	3	9	--	--	--	80
Sample 2012-2	4		3		--	4	--	--	10	--	--	11	5	62
Sample 2013-2 (Inside)	33	8	8	7	--	--	45	--	--	--	--	--	--	--
Sample 2013-2 (side 1)	26	9	2	6	--	--	58	--	--	--	--	--	--	--
Sample 2013-2 (side 2)	8	5		8	--	--	79	--	--	--	--	--	--	--
Sample 2013-3 (inside)	26		30	19	--	--	14	--	8	--	--	--	--	3
Sample 2013-3 (side 1)	30		16	29	--	--	19	--	3	--	--	--	--	3
Sample 2013-3 (side 2)	22		17	29	--	--	20	--	6	--	--	--	--	6
Archeologie 2013-6 (Inside)	5			25	5	--	52	1	7	--	--	--	--	6
Sample 2013-6 (side 1)	4		2	16	--	--	61	15	--	--	--	--	--	2
Sample 2013-6 (side 2)	9		4	21	--	--	57	5	--	--	--	--	--	3

The average composition of the corrosion products at each site is shown in Tab. 4. Magnetite was observed to be present as an anaerobic corrosion product even at those sites with low water content and easier oxygen transport.

Tab. 4 Average (normalised) composition of the corrosion products at the sites

Corrosion products (% by volume)	Magnetite	Hematite	Goethite	Lepidocrocite	Siderite	Total anaerobic	Total aerobic
SLANÝ	28	-	50	22	-	28	72
UTÍN	31	5	49	15	-	31	69
CHOMUTOV	25	1	53	21	-	25	75
ČEJKOV	29	-	43	29	-	29	71
OPATOV	11	-	83	6	-	11	89
TUCHOMĚŘICE	-	-	80	20	-	0	100
VELVARY	-	-	83	17	-	0	100
KONOPIŠTĚ	46	-	46	8	-	46	54
KUČEŘ	-	-	100	-	-	0	100
VRAŇANY	24	-	48	28	-	24	76
CHRBINA	18	16	58	8	-	18	82
LÍTOŽNICE	-	-	56	-	44	44	56
JIVINY	3	-	85	12	-	3	97
XAVEROV	-	-	100	-	-	0	100
ŽEHUŇ	40	6	44	1	9	50	50

Electron microscopy of perpendicular sections of corrosion products revealed interesting facts (see Fig. 6). Soil particles (visible on elemental maps as Si-rich sites or Al/Si mixtures) are mainly contained in the outer layer of corrosion products. The inner layer contains relatively homogeneous layers parallel to the surface, that are separated by pores (Fig. 7).

The pore space of bentonite is filled with corrosion products in the initial stage of deposition. This initial phase was also observed in short-term experiments in compacted bentonite. Once the transport of Fe cations is limited, the second phase begins with the preferential precipitation of corrosion products at the interface with the metal. Previously formed layers of corrosion products are forced out, and a new layer creates pressure from below. After reaching a certain thickness, the layer cracks and a new layer begins to form at the interface with the metal. Thus, while the first phase gradually slows down the corrosion attack over time, the second phase cyclically breaks the layer of corrosion products and thus the corrosion attack cyclically accelerates again. The second phase of attack evinces a semi-parabolic development pattern whereby the corrosion attack slows down within each cycle; however, over the long term it comprises a steady state with the linear dependence of the corrosion rate on the time, where the curve is formed by a constant decrease in the time.
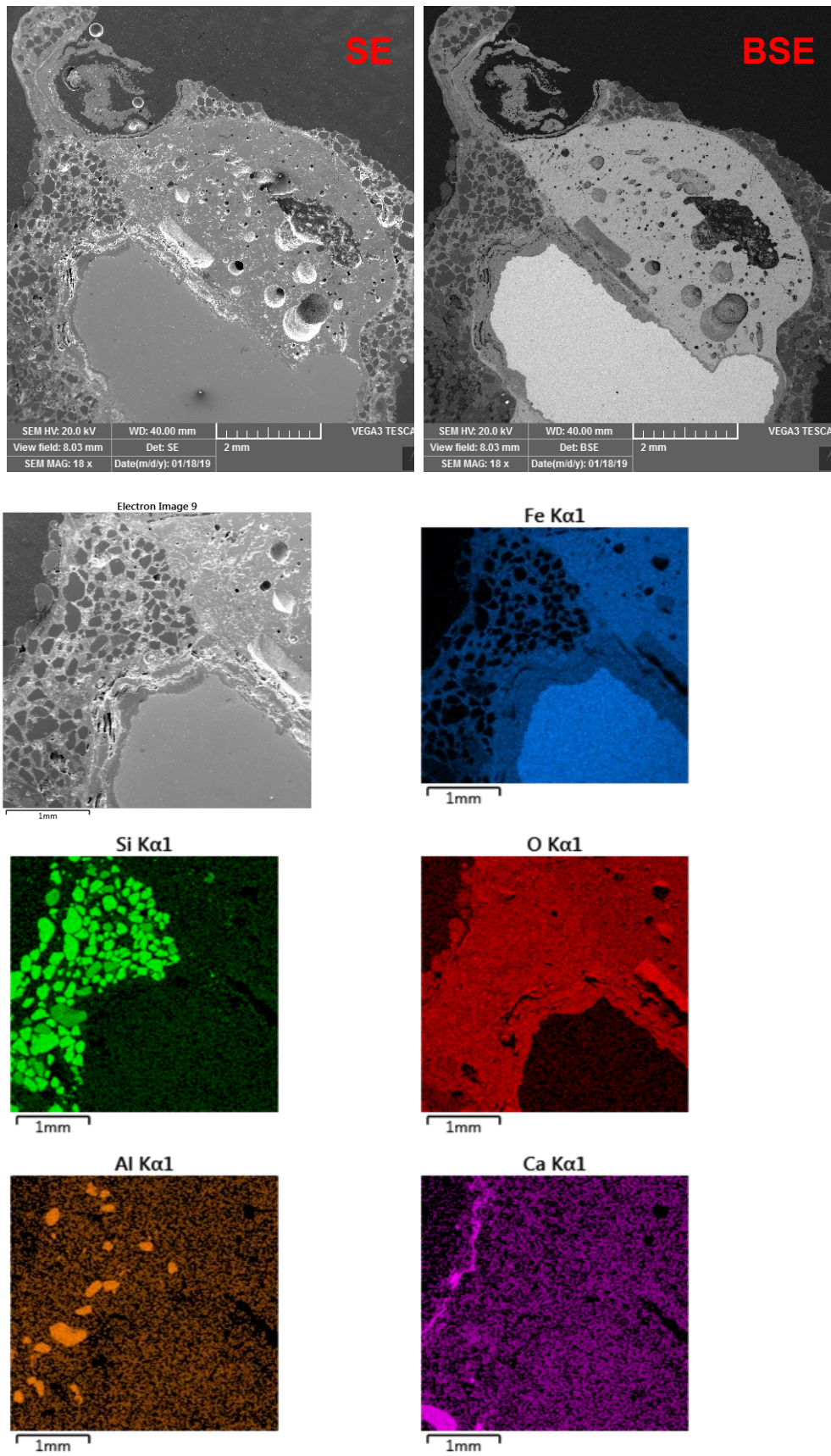
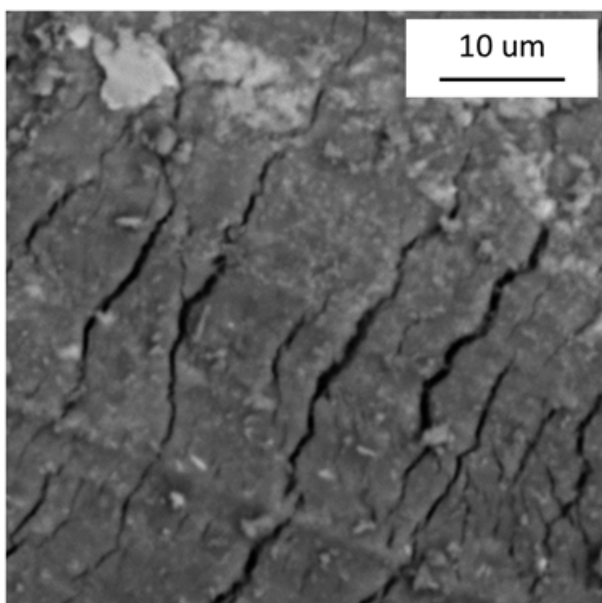Fig. 6 Electron microscope images with elemental maps.

Fig. 7 Example of internal layers of the corrosion products

The inner layers of the corrosion products were evaluated using samples where it was possible to consolidate the corrosion products by embedding them in epoxy resin under reduced pressure. Interestingly, regardless of the composition of the corrosion products, the thickness of this layer is remarkably constant for all sites and is around 3 μm (see Fig. 8). It is likely that the mechanical properties of the aggregates of the corrosion products are similar, thus, failure occurs at similar layer thickness.
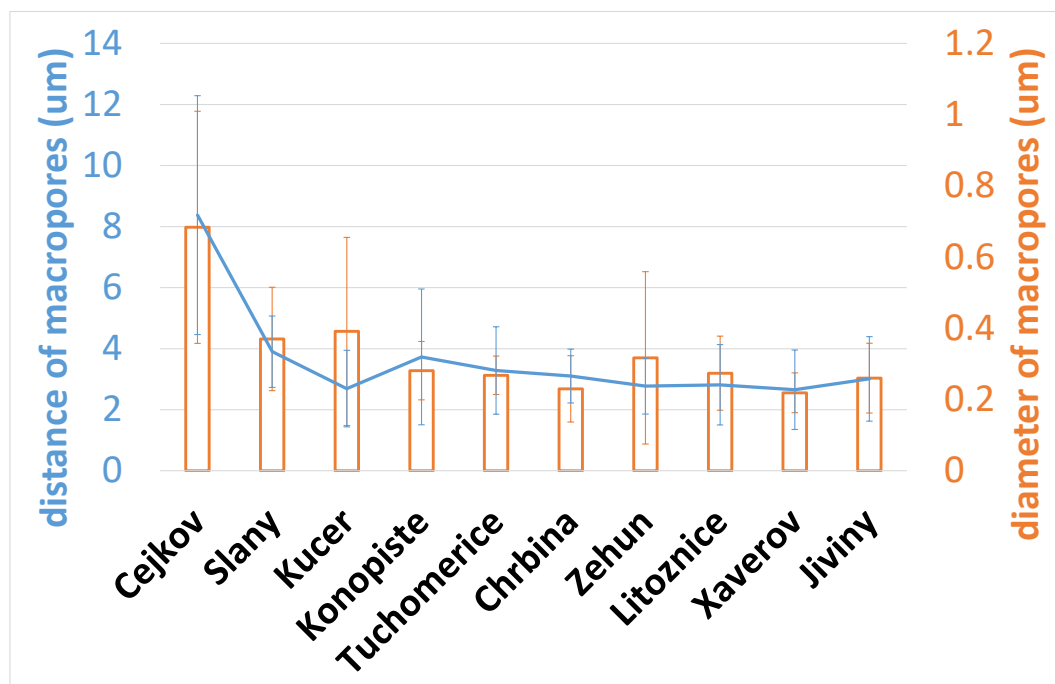

Fig. 8 Summary of the measurement results of the thicknesses of parallel inner layers of corrosion products and the diameters of the pores between them

Macroporosity was determined via digital image analysis of corrosion products supplemented by BET measurements, which allow to determine the meso- (pores between 50 and 2 nm) and microporosity (pores below 2 nm). While the macroporosity was observed to be more or less similar for all the samples, sites differ significantly in terms of the content of smaller pores (see Tab. 5). Mesopores are the main component at all sites, while the degree of microporosity is one order of magnitude lower. Sites in blue are those for which microporosity could not be determined on perpendicular sections, and a value of 2 (as the modus of the results) was taken for subsequent calculations.

Tab. 5 Porosity of the corrosion products

SITE	macroporosity (% by volume)	meso + microporosity (% by volume)
ČEJKOV	2	11
SLANÝ	3	18
KUČEŘ	7	15
KONOPIŠTĚ	2	12
TUCHOMEŘICE	2	17
CHRBINA	2	15
OPATOV	2	18
CHOMUTOV	2	22
VELVARY	2	18
UTÍN	2	7
ŽEHUŇ	4	16
LÍTOŽNICE	3	16
XAVEROV	2	17
JIVINY	2	1

Thanks to the selfless willingness of colleagues from the Faculty of Civil Engineering of CTU, an attempt was made to determine the mechanical properties of the corrosion products from the Žehuň site, which showed the best cohesion (see Appendix 4 for details). The corrosion products were found to be very easily deformable, their modulus of elasticity ranges from 8 to 52 GPa (Fig. 9). The blue line shows the greater level of stiffness of the corrosion products near the interface with the metal, which also indicates that the corrosion products in the inner layer were formed via precipitation in a smaller space than the initial outer layer. In order to determine the yield strength, it would be necessary to achieve a completely smooth surface at the abrasion point, which is very difficult for the aggregates and should be considered in future research in this direction.
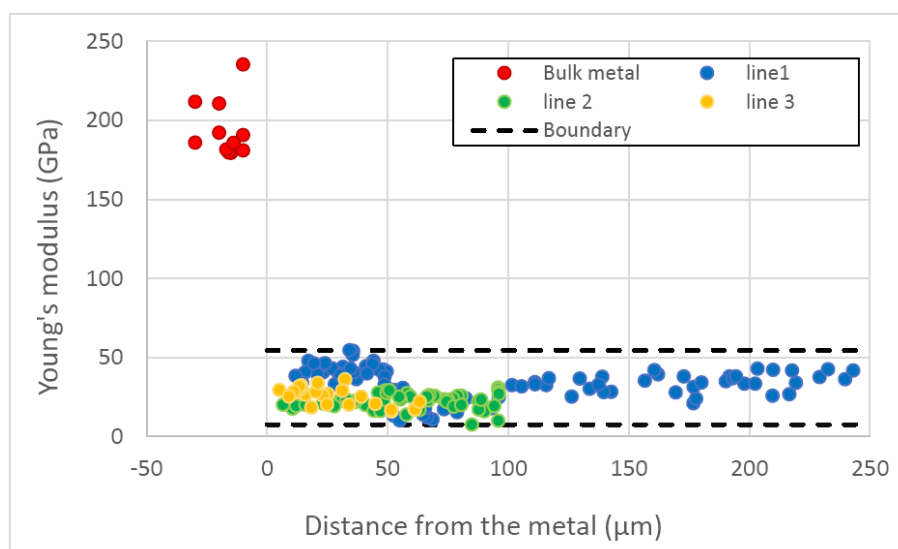
Fig. 9 Results of the nano-indentation measurements of the elastic modulus of corrosion products (red – indentation in the volume of ferrous metal; blue, yellow and green – indentation line profile at different positions in the corrosion products)

The procedure applied for correcting the volume of the corrosion products was as follows. The pore volume was subtracted from the total volume of the layer (Eq. 1). Subsequently, the volume of clay particles from the Rietveld analysis of the XRD data was subtracted from the solid part of the layer (Eq. 2).

$$V_{solid} = V_{total} - V_{por} \qquad\qquad\qquad\qquad\qquad\qquad\qquad\qquad\qquad Eq.\ 1$$

$$V_{copr} = V_{solid} - V_{clay} \qquad\qquad\qquad\qquad\qquad\qquad\qquad\qquad\qquad Eq.\ 2$$

(subscripts: TOTAL – total layer volume; POR – pore volume; SOLID – volume of the solid fraction; CLAY – clay soil particles; COPR – volume of corrosion products)

After subtracting the soil particles and porosity in the volume of the corrosion products layer volume, the corrosion products were converted with the help of densities (magnetite 5.00 g.cm^{-3}; siderite 3.87 g.cm-3; hematite 5.30 g.cm-3; goethite 4.30 g.cm-3; lepidocrocite 4.00 g.cm-3) to the amount of corroded metal (Tab. 6). Interestingly, corrosion is affected by soil porosity in a rather opposite way to that of the lifetime models based on short-term data, and higher corrosion rates are achieved by sites with lower soil porosity. Paradoxically, the sites with the least porous corrosion products have the highest corrosion rates. The lower porosity of the soil and, consequently, of the corrosion products hinders the transport of Fe cations and favours the precipitation of corrosion products at the interface with the metal and the earlier breakage of the corrosion products layer.

Tab. 6 Comparison of calculated corrosion penetration (loss) of metal with the soil porosity and the corrosion products

Site	Age (a)	Corrosion penetration (um)	Porosity of corrosion products (%)	Soil porosity (%)
ČEJKOV	600	525	13	47
TUCHOMĚŘICE	1500	337	19	48
SLANÝ	2600	2045	21	44
KONOPIŠTĚ	550	2526	14	41
KUCEŘ	500	1228	22	36
UTÍN	600	2782	9	-
VELVARY	1400	336	20	56
OPATOV	600	440	20	49
ŽEHUŇ	2100	749	20	44
JIVINY	2100	2159	3	34
XAVEROV	2000	770	19	35
LÍTOŽNICE	1600	1137	19	34

The following graph (Fig. 10) provides a comparison of all the data collected from the sites with the results of the original WDP project experiment, which was based on the precipitation of magnetite as the corrosion product (Forman et al., 2021); the model did not consider the cyclical mechanical failure of the corrosion products.
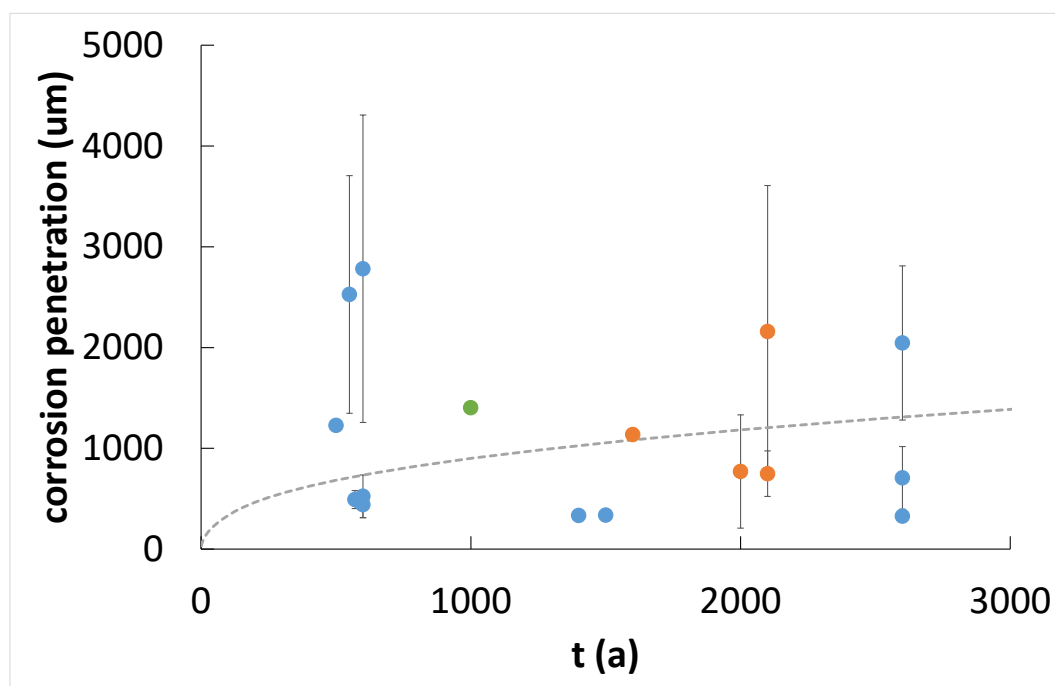

Fig. 10 Comparison of the data of the average value of the corrosion penetration to the depth of the iron (metal) with the original model as shown by the dashed line (the key, permanently watered sites are marked in orange; the Vraňany site, for which no complete porosity data was available, is marked in green; this indicator consists of a qualified estimate based on average values)

The probable evolution of the corrosion rate of the container over time is shown in Fig. 11. As indicated above, the first phase of corrosion product formation in an incompletely sealed bentonite pore system will be followed by a second phase with cyclic failure due to mechanical stress of the newly formed corrosion products.
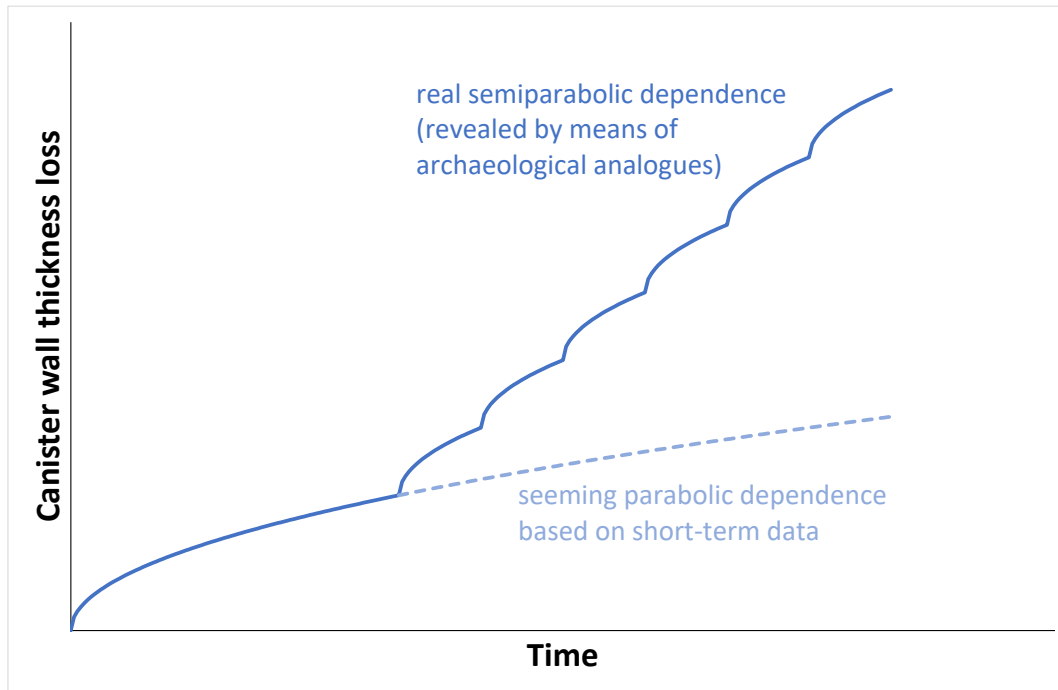

Fig. 11 Diagram of the evolution of the corrosion pumping life of the container

A model for the transport of oxygen through the soil pore system was proposed (Eq. 3) based on a steady diffusion flux (Fick's 1st law) and the assumptions that the kinetics of the oxygen reaction with metal/corrosion products on the surface are significantly higher, the process is driven by transport (which was, finally, confirmed retrospectively from the data in Tab. 7) and the concentration at the interface is close to zero. The equilibrium concentration of oxygen in an aqueous solution at a temperature of 11°C is 0.375 mol.m^{-3}.

$$J_{DIF} = \frac{D_{ef} \times c_b}{d} \qquad\qquad \textit{Eq. 3}$$

(legend: J_{DIF} – steady-state diffusion flux; D_{ef} – effective diffusion coefficient in the pore system of fully watered soils; c_b – oxygen concentration in the volume of the solution above the pore system; d – thickness of the pore system/ artifact deposition depth)

The effective diffusion coefficient in the soil pore system is based on the following relationships (Eqs. 4 and 5). The diffusion coefficient of oxygen in an aqueous solution at a temperature of 11°C is 1.3×10^{-9} m^2.s^{-1}. The values of constrictivity (0.35) and the empirical exponent β (1.4) used in the calculation of tortuosity are adopted from a study by (Leupin et al., 2021).

$$D_{ef} = D\,\frac{\Phi \times \delta}{\tau^2}$$

Eq. 4

(legend: D – diffusion coefficient in an aqueous solution; Φ – porosity; δ – constrictivity of the pore system; τ – tortuosity of the pore system)

$$\tau = \Phi^{-\beta}$$

Eq. 5

(legend: β – empirical exponent)

From the results (Table 7) is evident that the contribution of aerobic corrosion (supplied electrons for corrosion processes) is minimal and the oxidation to higher oxidation states of corrosion products must have occurred only during the pick-up due to slow drying and contact with the atmosphere.

Tab. 7 Result of the theoretical model of the transport of oxygen to the surface of the artifacts and its contribution to corrosion attack

| | | | | | | Electrons consumed for corrosion to the oxidation state of the corrosion products. (mol.m^{-2}) | | | | |
| | | | | | | magnetite | hematite | goethite | lepidocrocite | siderite |
Site	Porosity	D_{eff} (m^2.s^{-1})	Depth (m)	Age (a)	Electrons supplied by oxygen (mol.m^{-2})					
ŽEHUŇ	0.439	1.99E-11	0.25	2100	8	69	18	191	3	18
LÍTOŽNICE	0.342	7.71E-12	0.30	1600	2	0	0	312	0	113
XAVEROV	0.351	8.51E-12	0.15	2000	5	0	0	326	0	0
JIVINY	0.336	7.21E-12	0.40	2100	2	11	0	797	70	0

The original models assumed the uniform distribution of cations for the formation of the corrosion products both epi- and topotactically and the zero mechanical loading of the inner layer of corrosion products. However, it appears that the distribution of cations between the two interfaces shifts significantly in favour of the inner interface, especially in the second phase of development (see the diagram in Fig. 11), and that subsequent precipitation causes much earlier failure of the layer of corrosion products.

Concerning subsequent modelling in this respect, it will be necessary to add data on the precipitation kinetics, porosity and mechanical properties (including strength and critical bending deformation) of the corrosion products.

At present, only an empirical evaluation of the effect on durability, assuming identical discrete time dependence of the layer evolution on time (semi-parabolic dependence), can be seriously performed. The slowdown in the formation of this layer has no effect in the long term and can be approximated by a linear dependence. Two fully watered sites, Jiviny and Xaverov were selected.

Both sites provide a statistically significant amount of data (which was not the case for the Lítožnice site) and no original layer of mica was detected on the surfaces (as at the Žehuň site). The Jiviny site is extreme in terms of the low porosity of the corrosion products, whereas the Xaverov site evince normal corrosion products porosity.

The lifetime of the container with a corrosion allowance of 15 mm would be 6,230 years according to the data from the Jiviny site and 15,840 years according to that obtained from the Xaverov site. Even in the case of such extreme estimate, the lifetime of the outer containment is sufficient and exceeds the minimum period of 2,600 years (Kotnour et al., 2016). It should be emphasized, however, that the determination of the lifetime, once the necessary parameters for the environment and corrosion products of the repository are determined, may vary, but probably to higher times.

3 Conclusion

Data were obtained from 15 archaeological sites and more than 200 artifacts. 4 sites showed complete and continuous waterlogging, as they were pond bottoms. The other sites had incomplete pore filling and cycled with precipitation and ambient temperature.

Chemically, the pore solutions from all sites are very similar to bentonite. Nevertheless, unlike bentonite pore solutions, there is a preferential formation of corrosion products based on iron oxides and hydroxides rather than carbonates, as has been experimentally observed in anaerobic bentonite environments. According to thermodynamic models, this is probably due to the partial access of oxygen, since the formation of siderite is linked to an environment with a very low redox potential (completely anaerobic environment) and lower pH. An important observation is that even after exposure over hundreds to thousands of years, the formation of silicate corrosion products was not observed, despite the high concentration of dissolved silicates.

The evaluation of corrosion products showed that after an initial period, when corrosion products form in the pore system of the surrounding soil, there is a period when, after sufficient sealing of the pore system, there is preferential formation of corrosion products at the interface with the metal and cyclic failure of the entire layer of corrosion products. The evaluation of the kinetics of the corrosion process showed that the original shape of the parabolic dependence of corrosion penetration on time transitions to a semiparabolic (linear) shape during this period. Thus, the previous lifetime assessment based on short-term data is incomplete and only includes the initial period of lifetime evolution. Extrapolated lifetimes based on short-term data were on the order of 10^6 years (Forman et al., 2021). Based on this project, the corrected lifetimes of the carbon steel outer shell can be estimated in the order of 10^4 years. However, this lifetime is sufficient because the main barrier of the container is the stainless steel inner casing, which will provide the required lifetime of one million years. The outer casing only needs to survive the initial period of storage before oxygen is consumed and the temperature drops to 40 °C to ensure a stable passive layer on the surface, which is 2,600 years with the current knowledge of the evolution of conditions in deepwater storage (Kotnour et al., 2016).

The mechanical properties of corrosion product aggregates are obviously very poor based on modulus of elasticity measurements, allowing them to be easily broken. On the other hand, the easy deformability and high porosity give hope that concerns about whether newly formed corrosion products with a volume greater than the original metal may contribute to the ambient pressure acting on the container are probably unfounded.

An experimental study focusing on the mechanical properties and porosity of carbonate corrosion products formed in a strictly anaerobic compacted bentonite environment will be needed to further refine the lifetime determination. Another important piece of information is the time-varying distribution ratio of new precipitates in the corrosion product layer.

References

FORMAN L., PICEK M. DOBREV D., GONDOLLI J., MENDOZA MIRANDA A.N., STRAKA M., KOUŘIL M., STOULIL J., MATAL O., ČERMÁK J., KRÁL L., ŽALOUDEK J., VÁVRA M, ČUPR M. (2021): Závěrečná technická zpráva výzkumná část projektu Výzkum a vývoj ukládacího obalového souboru pro hlubinné ukládání vyhořelého jaderného paliva do stadia realizace vzorku, Praha, ZZ 544/2021

KOTNOUR P., PECHMANOVÁ E., MATOUŠEK J., LOVECKÝ M., ŠIK J., DOBREV D., GONDOLLI J., KÁRNÍK D., KOUŘIL M., STOULIL J., MACÁK P., MATAL O., ČERMÁK J., KRÁL L. ŽALOUDEK J., VÁVRA M., ČUPR M. (2016): Průběžná technická zpráva 2. etapa – ŠKODA JS a.s. Plzeň, SÚRAO 402/2019

LEUPIN, O. X., SMART, N. R., ZHANG, Z., STEFANONI, M., ANGST, U., PAPAFOTIOU, A. & DIOMIDIS, N. 2021. Anaerobic corrosion of carbon steel in bentonite: An evolving interface. Corrosion Science, 187.